Excellent surface enhanced Raman scattering obtained with nanoporous gold fabricated by chemical de-alloying

Excellent surface enhanced Raman scattering obtained with nanoporous gold fabricated by chemical de-alloying

Yanpeng Xue, Federico Scaglione, Eirini Maria Paschalidou, Paola Rizzi, Livio Battezzati
Dipartimento di Chimica e Centro Interdipartimentale NIS (Nanostructured Surfaces and Interfaces), Università di Torino, Via Pietro Giuria 7, 10125 Torino, Italy

ABSTRACT

Three dimensional nanoporous gold, with an average ligament size of 50 nm, was fabricated by chemical de-alloying from a new Au based metallic glass precursor. The resultant nanoporous gold gives rise to superior surface enhanced Raman scattering (SERS) capability using 4,40-bi-pyridine as probe molecules. The SERS intensity mapping images confirm the presence of hot spots. A low detection limit down to 10 14 M for bipyridine was achieved, which is attributed to the localized enhanced electromagnetic fields around nano-sized ligaments, the electromagnetic coupling between ligaments, and the trapped SERS sensitive atoms.

1. Introduction

Surface enhanced Raman scattering (SERS) is a promising tech-nique in probing and identifying trace level molecules in chemical and biological systems owing to its high molecular specificity and high sensitivity [1,2]. Single molecular detection was demon-strated using molecules with high effective cross sections and sub-strates with high density of adequate sites [3,4]. It was recognized that the strong SERS enhancement was due to the chemical effect with the contribution of about two orders of magnitude [5], and the dramatic electromagnetic effect arising from the resonant exci-tation of localized surface plasmons in the vicinity of the metallic surface [6]. The electromagnetic field enhancement is strongest at sharp edges or tips [7], interparticle gaps [3,8] and nanopores [9], typically referred as ‘‘hot spots”. To date, various substrates have been tested for high performance SERS, for examples period-ical micropillar arrays prepared by lithography [1], self-organizations of nanoparticles [10,11], and nanoporous substrates [9]. Among them, nanoporous gold with a bicontinuous network structure has recently been exploited as an attractive substrate for SERS applications [12,13]. The SERS enhancement of the gold ligaments is attributed to the large curvatures of the nanoscaled ligaments and nanopores [14], as well as the electromagnetic cou-pling between the neighbouring ligaments [15].

Many strategies have been proposed to fabricate nanoporous gold, among which the de-alloying method by free corrosion or electrochemical de-alloying has become one efficient way. During the de-alloying process, the less noble elements of a precursor alloy are selectively dissolved, while the noble metal atoms reorga-nize into interconnected open-pore structure at the metal-electrolyte interfaces by surface diffusion [16,17]. The precursors for de-alloying can be either crystalline alloys or metallic glasses. When the precursor is a crystalline alloy, each grain in the microstructure remains the original orientation after de-alloying and becomes a porous single crystal [18]. Compared with crys-talline alloys, metallic glass precursors in principle are monolithic as a phase with a homogeneous composition and structure free from grain boundaries and other crystalline defects. Therefore, the metallic glass precursor could be a better choice to obtain a uniform nanoporosity by the de-alloying method. However, due to the higher corrosion resistance of metallic glasses compared with crystalline alloys, proper de-alloying conditions are needed to get a continuous network of ligaments and pores and to avoid cracks and stress corrosion cracking [19,20]. During the de-alloying process from metallic glass precursors, the nucleation and growth of crystals must occur to form ligaments [21,22].

In a previous work, nanoporous gold was prepared by electro-chemical de-alloying from the $Au_{30}Cu_{38}Ag_7Pd_5Si_{20}$ metallic glass precursor with ligament size ranging from 75 to 200 nm showing it is a good substrate for surface enhanced Raman scattering, with a detection limit of 10^{11} M using bipyridine as probe molecule [23]. In this study, we report that nanoporous gold was fabricated from a new $Au_{20}Cu_{48}Ag_7Pd_5Si_{20}$ (at.%) metallic glass precursor by chemical de-alloying and used as substrate for surface enhanced Raman scattering with high sensitivity.

2. Experimental

A $Au_{20}Cu_{48}Ag_7Pd_5Si_{20}$ (at.%) master alloy was prepared by arc melting the pure elements (Au: 99.99%, Ag, Cu, Pd: 99.99%, Si: 99.9995%) in Ti-gettered Argon atmosphere. The ingot was rapidly solidified onto a rotating copper wheel at a linear speed of 25 m/s. The thickness of the resulting ribbon is around 25 lm and the width is around 2 mm. Chemical de-alloying of the as-spun ribbons was conducted in concentrated HNO_3 (65% volume) and 0.5 M HF at room temperature. After de-alloying, the as-dealloyed samples were rinsed with distilled water and then dried for investigation. The surface morphology of de-alloyed samples was observed by Scanning Electron Microscopy (SEM) and their compositions were checked by Energy Dispersive X-ray Spectroscopy (EDS) after Co calibration. The structure of the materials was studied by X-ray Diffraction (XRD) using Cu K_a wavelength in Bragg-Brentano mode.

Micro-Raman measurements were performed with a Renishaw inVia Raman Microscope using 785 nm laser line with an acquisi-tion time of 20 s, 0.05% power at the sample and a 50 ULWD objective; 4,4^0-bipyridine (bipy) was chosen as SERS probe mole-cules [24]. Prior to SERS experiments, the nanoporous gold samples were cleaned in concentrated nitric acid for 5 min and rinsed several times in de-ionized water. The samples were immersed in the etha-nol solution of 4,4^0-bipyridine with concentrations from 10^{11} M to 10^{14} M for one night, enabling the probe molecules to be adsorbed on the surface. Measurements were performed on the surface of sample after drying at air. SERS intensity Mapping images have been collected in a 24 24 lm^2 area with bipyridine concentration of 10^{12} M and 10^{14} M based on characteristic peak at 1614 cm^{1} under the same condition of single measurement. All solutions were prepared from chemical grade reagents and de-ionized water.

3. Results and discussion

The alloy $Au_{20}Cu_{48}Ag_7Pd_5Si_{20}$ (at.%) has been developed with lower Au content with respect to previous reports to lower the cost and to achieve finer microstructure of the de-alloyed materials [23,25]. Fig. 1 shows the XRD patterns of as-spun $Au_{20}Cu_{48}Ag_7Pd_5$-Si_{20} (at.%) ribbon and the de-alloyed sample in concentrated HNO_3 and 0.5 M HF at room temperature for 3 days. The XRD pattern of the as-spun ribbon illustrates the characteristic broad halo indica-tive of its amorphous structure. After chemical de-alloying for

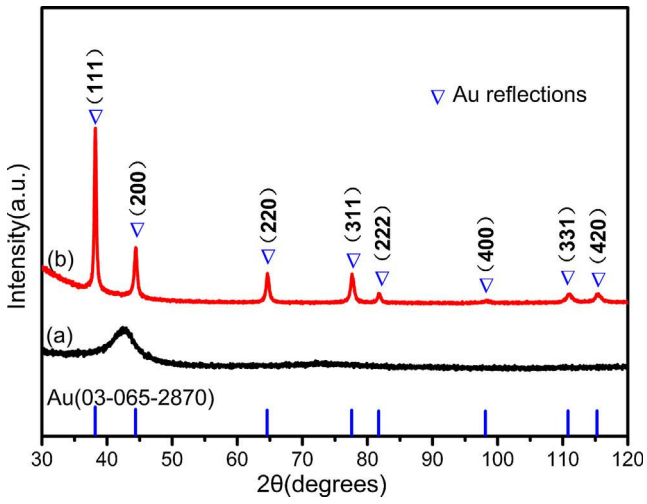

Fig. 1. XRD patterns of (a) the as-spun $Au_{20}Cu_{48}Ag_7Pd_5Si_{20}$ (at.%) ribbon and (b) sample de-alloyed in mixture of concentrated HNO_3 and 0.5 M HF at room temperature for 3 days.

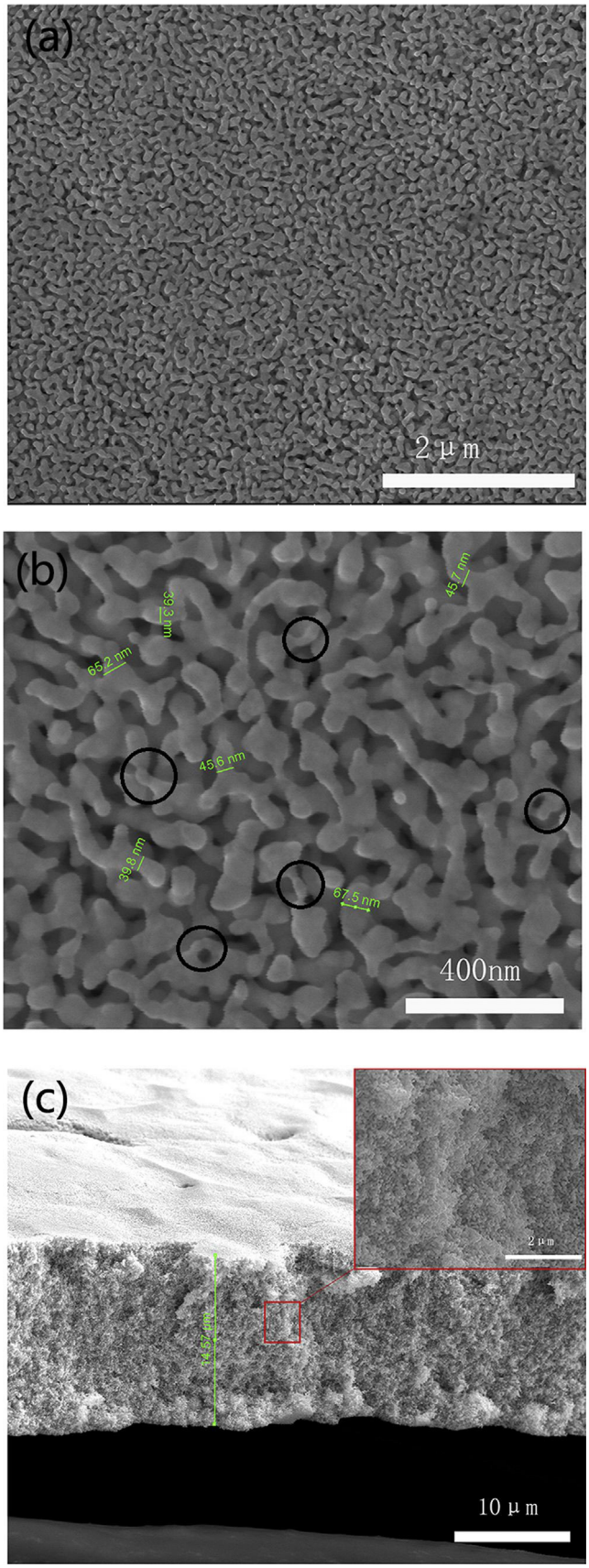

Fig. 2. (a) Microstructure of as-dealloyed sample in mixture of concentrated HNO_3 and 0.5 M HF at room temperature for 3 days. (b) Enlarged image of (a) showing an average ligament size of around 50 nm. (c) Cross section of as-dealloyed sample. The inset shows the enlarged image of marked red rectangle.

3 days, the amorphous broad halo disappears completely and sharp crystalline reflections form representative of the face-centered cubic Au.

The microstructure of the nanoporous gold was observed by SEM and its compositions were analyzed by EDS. Fig. 2 shows SEM images of surface and cross section of the ribbons obtained by chemical de-alloying of $Au_{20}Cu_{48}Ag_7Pd_5Si_{20}$ metallic glass precursor in mixture of concentrated HNO_3 and 0.5 M HF at room temperature for 3 days. After chemical de-alloying, a bicontinuous nanoporosity throughout the sample was obtained and the ribbon has been de-alloyed in three dimension scale. Large pores exist randomly on the surface (Fig. 2a). From the high magnification image (Fig. 2b), the size of ligaments measured at their narrower necks ranges from 40 to 70 nm while, occasionally, narrow ligaments around 25 nm have been measured and marked with circles. The average size resulting from at least one hundred ligaments, has been evaluated being 50 ± 10 nm (scat-ter is one standard deviation in the size distribution). The ligament surface is rough and the ligaments are composed of several crystals: this morphology is mainly the result of the dealloying mechanism occurring in amorphous alloys. In addition with the progressive removal of less noble elements, Au adatoms freed on the surface and driven by surface diffusion, aggregate forming crystalline domains. These grow as a function of the time until they impinge with other domains forming ligaments [21].

The microstructure obtained by free corrosion is finer compared with nanoporous gold prepared from $Au_3LCu_{38}Ag_7Pd_5Si_{20}$ (at.%) metallic glass precursor; in that case the size of ligaments is around 200 nm after electrochemically de-alloying at 70 LC in 1 M HNO_3 for 6 h [23] (For the detailed comparison between this two alloys, see supporting information S1). The tiny nanoporous structure is attributed to reduced supply of Au adatoms during the de-alloying process because of the lower content of gold in metallic glass precursor. From the cross section of the as-dealloyed sample, the thickness of the ribbon decreases from 25 lm to 15 lm because the 80% of the less noble elements were removed from the precursor. Further analyses of the nanoporous structure (see inset in Fig. 2c) imply that the ligament sizes in the cross section are around 50 nm, which is consistent with those observed on the surface, demonstrating the uniformity of the nanoporous structure. From the EDS quantitative analysis, the composition of the original specimen is close to the nominal one while the nanoporous gold is mainly composed of Au with traces of Ag and Pd. Under free corrosion conditions, the driving force for chemical de-alloying is the large differences of electrochemical potential between components which result in the removal of less noble elements from the metallic glass precursor. From the EDS quantitative data, one can see that the a limited amount of less noble elements has been trapped in the newly formed ligaments.

In order to demonstrate the SERS capability of the resulting nanoporous gold, 4,4^0-bipyridine (bipy) was selected as probe molecule. The SERS effect of ribbons chemically de-alloyed for 3 days was tested after immersing them for one night in ethanol

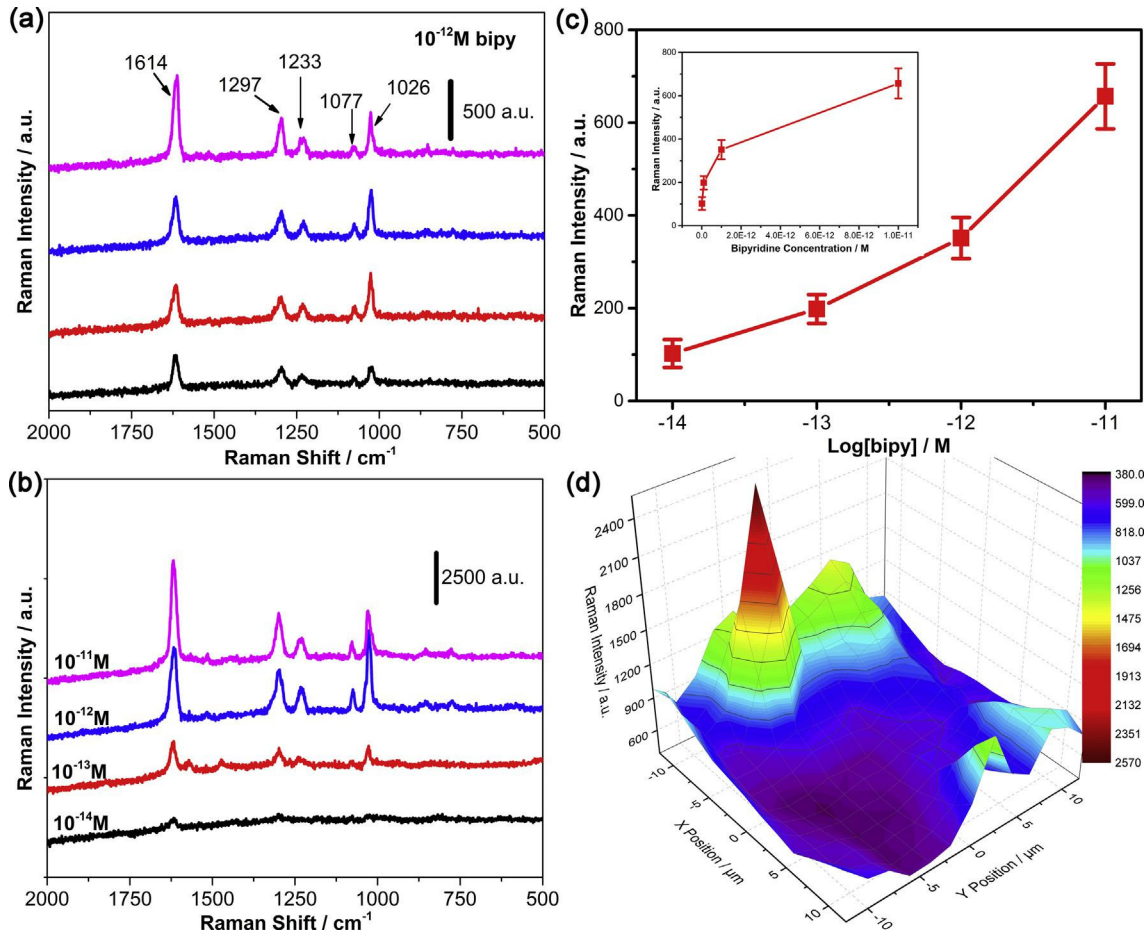

Fig. 3. (a) SERS spectra of 10 ^{12} M 4,4^0 -bipyridine at different sites on a de-alloyed sample. (b) SERS spectra of 4,4^0 -bipyridine with 10 accumulations at different concentrations on de-alloyed samples. (c) Relationship between the SERS intensity at 1614 cm ^{1} and the logarithm of bipyridine concentration. Inset shows SERS intensity at 1614 cm ^{1} as a function of bipyridine concentrations. The error bars were calculated from at least 10 measurements on random spots on the same substrate. (d) SERS intensity mapping image of 24 24 lm^2 with bipyridine concentration of 10 ^{14} M based on characteristic peak at 1614 cm ^{1}. The laser wavelength was 785 nm with an acquisition time of 20 s for single measurement.

solution of bipyridine with different concentrations in the range 10^{-11}–10^{-14} M bipyridine. After de-alloying ribbons are easy to handle with tweezers, being bendable and free standing. This good mechanical stability of samples is very favorable for a substrate in SERS application.

Fig. 3(a) shows the SERS spectra excited by a 785 nm laser at different sites randomly selected on both sides after one night immersion in 10^{-12} M bipyridine solution. The characteristic peaks of bipyridine are easily discerned at 1614, 1297, 1233, 1077 and 1026 cm^{-1}, which are in good agreement with the literature [24,26]. The spectra variation in the relative intensity and band width can be observed at different sites, which are associated with the orientation and adsorption kinetics of molecules as well as the electromagnetic field variation at each ‘‘hot spot” [7]. The Raman spectra shown in Fig. 3b are the most intense ones with 10 accu-mulations for each concentration under the same experimental conditions. It is noted that the characteristic peaks of bipyridine are still visible even when the solution concentration is diluted to 10^{-13} M. When the concentration is further decreased of one order of magnitude, i.e. 10^{-14} M, peaks of the probe molecule are strongly weakened but still recognizable, therefore the detection limit concentration of bipyridine on the surface of this nanoporous gold can be as low as 10^{-14} M. Compared with nanoporous gold prepared by electrochemical de-alloying from the $Au_{30}Cu_{38}Ag_7Pd_5$-Si_{20} metallic glass precursor with a detection limit of 10^{-11} M using bipyridine as probe molecules, our substrate shows excellent SERS sensitivity under the same measurement conditions. Fig. 3c shows the relationship between SERS intensity at 1614 cm^{-1} and bipyri-dine concentration; the error bars show the variation of magnitude of intensity at each concentration. The inset shows that the detec-tion limit is approached with decreasing the bipyridine concentra-tion. Fig. 3d shows SERS intensity mapping image with bipyridine concentration of 10^{-14}M under the same condition of single mea-surement, which confirms the presence of ‘‘hot spots”. A mapping image with bipyridine concentration of 10^{-12} M is available on the supporting information S2. From SERS intensity mapping images it is clear that the hot spots are present, but not homogenously dis-tributed on the substrate surface.

The enhancement of SERS effect on nanoporous gold mainly arises from local electromagnetic field enhancement caused by plasmon excitation of ligaments through incident laser light. From Fig. 2b, the bicontinuous structure of nanoporous gold consists of ligaments with average size of 50 nm. And there are many of nar-row ligaments around 25 nm. The Raman ‘‘hot spots” are typically generated at these locations, where local electromagnetic fields are dramatically enhanced because of the resonant excitation of local-ized surface plasmons. This is in agreement with the results of Chen’s group that the SERS intensity of nanoporous gold is dramat-ically enhanced with decreasing ligament size [15]. Also, the elec-tromagnetic coupling effect between adjacent gold ligaments may further enhance the localized field intensity, leading to further improvement of the SERS enhancement [15]. Furthermore from the EDS quantitative analysis, the nanoporous gold retains a small amounts of Ag and Pd atoms, which are trapped inside ligaments during de-alloying process. The residual Ag and Pd atoms con-tributes significantly to the SERS enhancement of nanoporous gold [23,27].

4. Conclusions

In summary, we fabricated nanoporous gold by chemical de-alloying from newly developed Au based metallic glass precursor. The resultant nanoporous gold exhibited superior surface enhanced Raman scattering capability with detection limit down to 10^{-14} M for bipyridine. The SERS intensity mapping images with bipyridine concentration of 10^{-12} M and 10^{-14} M confirm the pres-ence of hot spots. The strong SERS enhancement is attributed to the localized enhanced electromagnetic fields around nano-sized liga-ments, the electromagnetic coupling between ligaments, and the trapped SERS sensitive atoms. This biocompatible and easy to han-dle SERS active substrate with high sensitivity has great potential in application of ultrasensitive instrumentation for molecule diag-nostics [7,28].

Acknowledgements

Dr. Alessandro. Damin is kindly acknowledged for the SERS experiments. This work was supported by the funding scheme of the European Commission, Marie Curie Actions - Initial Training Networks (ITN) in the frame of the project VitriMetTech - Vitrified Metals Technologies and Applications in Devices and Chemistry, 607080 FP7-PEOPLE-2013-ITN.

Appendix A. Supplementary material

Supplementary data associated with this article can be found, in the online version, at http://dx.doi.org/10.1016/j.cplett.2016.10. 046.

References

[1] F. De Angelis, F. Gentile, F. Mecarini, G. Das, M. Moretti, P. Candeloro, M.L. Coluccio, G. Cojoc, A. Accardo, C. Liberale, R.P. Zaccaria, G. Perozziello, L. Tirinato, A. Toma, G. Cuda, R. Cingolani, E. Di Fabrizio, Nat. Photonics 5 (2011) 682–687.

[2] M.P. Cecchini, V.A. Turek, J. Paget, A.A. Kornyshev, J.B. Edel, Nat. Mater. 12 (2012) 165–171.
[3] S. Nie, S.R. Emory, Science 275 (1997) 1102–1106.
[4] K. Kneipp, Y. Wang, H. Kneipp, L.T. Perelman, I. Itzkan, R.R. Dasari, M.S. Feld, Phys. Rev. Lett. 78 (1997) 1667–1670.
[5] S.M. Morton, L. Jensen, J. Am. Chem. Soc. 131 (2009) 4090–4098.
[6] N.P.W. Pieczonka, R.F. Aroca, Chem. Soc. Rev. 37 (2008) 946–954.
[7] L. Zhang, H. Liu, L. Chen, P. Guan, B. Chen, T. Fujita, Y. Yamaguchi, H. Iwasaki, Q.-K. Xue, M. Chen, RSC Adv. 6 (2016) 2882–2887.
[8] D.-K. Lim, K.-S. Jeon, J.-H. Hwang, H. Kim, S. Kwon, Y.D. Suh, J.-M. Nam, Nat. Nanotechnol. 6 (2011) 452–460.
[9] X. Zhang, Y. Zheng, X. Liu, L. Wei, J. Dai, D.Y. Lei, D.R. MacFarlane, Adv. Mater. 27 (2015) 1090–1096.
[10] W. Niu, Y.A.A. Chua, W. Zhang, H. Huang, X. Lu, J. Am. Chem. Soc. 137 (2015) 10460–10463.
[11] J.W. Hong, S.U. Lee, Y.W. Lee, S.W. Han, J. Am. Chem. Soc. 134 (2012) 4565– 4568.

[12] S.O. Kucheyev, J.R. Hayes, J. Biener, T. Huser, C.E. Talley, A.V. Hamza, Appl. Phys. Lett. 89 (2006) 053102.
[13] L.H. Qian, X.Q. Yan, T. Fujita, A. Inoue, M.W. Chen, Appl. Phys. Lett. 90 (2007) 153120.
[14] X.Y. Lang, L.Y. Chen, P.F. Guan, T. Fujita, M.W. Chen, Appl. Phys. Lett. 94 (2009) 213109.
[15] X. Lang, P. Guan, L. Zhang, T. Fujita, M. Chen, J. Phys. Chem. C 113 (2009) 10956–10961.
[16] J. Erlebacher, M.J. Aziz, A. Karma, N. Dimitrov, K. Sieradzki, Nature 410 (2001) 450–453.
[17] J. Erlebacher, J. Electrochem. Soc. 151 (2004) C614–C626.
[18] S. Van Petegem, S. Brandstetter, A.M. Hodge, B.S. El-Dasher, J. Biener, B. Schmitt, C. Borca, H. Van Swygenhoven, Nano Lett. 9 (2009) 1158–1163.
[19] H.W.P.J.D. Fritz, B.W. Parks, Scr. Metall. 22 (1988) 1063–1068.
[20] G.S. Duffó, S.B. Farina, J.R. Galvele, Corros. Sci. 46 (2004) 1–4.
[21] F. Scaglione, F. Celegato, P. Rizzi, L. Battezzati, Intermetallics 66 (2015) 82–87.
[22] M. Zhang, A.M. Jorge Junior, S.J. Pang, T. Zhang, A.R. Yavari, Scr. Mater. 100 (2015) 21–23.
[23] F. Scaglione, E.M. Paschalidou, P. Rizzi, S. Bordiga, L. Battezzati, E.M. Paschalidou, P. Rizzi, S. Bordiga, L. Battezzati, Philos. Mag. Lett. 95 (2015) 474–482.

[24] S.W. Joo, Vib. Spectrosc. 34 (2004) 269–272.
[25] F. Scaglione, P. Rizzi, F. Celegato, L. Battezzati, J. Alloys Compd. 615 (2014) S142–S147.
[26] M. Suzuki, Y. Niidome, S. Yamada, Thin Solid Films 496 (2006) 740–747.
[27] L. Zhang, L. Chen, H. Liu, Y. Hou, A. Hirata, T. Fujita, M. Chen, J. Phys. Chem. C 115 (2011) 19583–19587.
[28] H. Liu, L. Zhang, X. Lang, Y. Yamaguchi, H. Iwasaki, Y. Inouye, Q. Xue, M. Chen, Sci. Rep. 1 (2011) 1–5.